

Chapter 1

Physical Ideas Underlying SPAM

/ Motivation / Particles *versus* Continua / Newton's Particle Mechanics / Eulerian and Lagrangian Continuum Mechanics / Microscopic Computer Simulation [Molecular Dynamics] / Statistical Mechanics / Macroscopic Particle Simulation / SPAM /

/ **7 Figures** /

Example Problem :

[Molecular Dynamics—Leapfrog and Runge-Kutta Methods]

1.1 Motivation and Summary

The flow of fluids, the deformation of solids, the design of structures able to withstand large and rapid loads, the analysis of complex failure mechanisms—all of these require numerical simulation techniques. Typical interesting problems of these types are nonlinear, and often “chaotic” as well, meaning that the evolving numerical solutions are exponentially sensitive to small changes in the initial conditions. SPAM is a simple and flexible numerical technique. It has developed so as to address the need for efficient designs of structures responding to rapid loading and for reliable analyses of fluid and solid flows and deformations.

Smooth Particle Applied Mechanics, “SPAM” for short, is a very general approach to the simulation of bulk matter in motion. Its novelty lies in a clever method for smooth interpolation and differentiation within an irregular grid of moving particles. The emergence of SPAM is a natural consequence of the fast high-capacity computers which make it possible to

attack complex numerical problems. Computers feed on *algorithms*, concrete numerical recipes¹ which can closely approximate the abstract mathematical ideas used to model and to analyze material motion. The last three centuries have seen Newton's analysis of particle motions governed by "action at a distance" abstracted to Euler and Lagrange's analyses of continua composed of unseen mutually interacting particles. The partial differential field equations of continuum mechanics, which include both time and space derivatives, can place heavy demands on digital computers, which are necessarily restricted to a finite number of variables described with finite precision.

Approximating the solution of the partial differential equations describing continuum problems by using *particles*, not atoms but *macroscopic* particles, is a clever idea. Clever ideas in physics often exhibit redundancy, showing up nearly simultaneously in more than one place. In 1977, after about 30 years of computer simulation, physics was ripe for the application of *particle* simulations to *continuum* problems. And it happened then that Gingold, Lucy, and Monaghan discovered the smooth-particle approach to continuum simulations while working at Cambridge University. Their joint discoveries of this new approach resulted from confronting challenging astrophysical problems. Gingold and Monaghan were interested in modeling rotating stars. They found that on the order of one hundred particles provided semiquantitative structural descriptions of such rotating bodies, including both gravitational and magnetic fields.² Lucy was likewise interested in rotating stellar matter, but beyond the stability limit. He was able to explain the production of close binary pairs of stars by following the detailed breakup of rotating masses, likewise represented by about one hundred particles.³ These early calculations demonstrated the ability of smooth particle techniques to deal with longrange gravitational forces. The electric and magnetic field forces found in plasma physics and magnetohydrodynamics can likewise be dealt with, but require special techniques which are unnecessary for the mechanical problems stressed in this book.

For those accustomed to precise analytic solutions the necessarily approximate nature of SPAM solutions might be disconcerting. The errors incurred, usually of the order of a few percent, are quite an acceptable price to be paid in exchange for the ability to solve hard nonlinear problems with a relatively simple and transparent method. The present book

¹Press, Flannery, Teukolsky, and Vetterling, *Numerical Recipes* (1986).

²Gingold and Monaghan (1977).

³Lucy (1977).

is an elaboration and illustration of the refinement of these earlier ideas to applications in fluid and solid mechanics rather than to astrophysics. Numerical continuum problems are considered here in the context of our developing knowledge of particle mechanics, which has recently been enriched by ideas taken from chaos theory and from nonlinear dynamics.⁴ All the numerical methods discussed here will continue to profit from increases in computational speed and capacity.

Here we begin with a summary of classical mechanics, from Newton up until the development of fast computers. This foundation is followed by a quick tour of computational developments, spanning the last half century, which have made it possible to flesh out the earlier theoretical developments with numerical examples.

1.2 Particles versus Continua

Matter can be described by either particle mechanics or continuum mechanics. The two approaches are quite different, both in the underlying assumptions, and in the forms of the results obtained. Particle mechanics, as described in the next Section, and as illustrated in an Example Problem at the end of this Chapter, uses *ordinary* differential equations for $r(t)$ to evolve particle trajectories. The underlying assumption is the functional form of the force law on which the motion depends. No constitutive information (equilibrium equation of state and nonequilibrium transport laws) needs to be specified. All such information follows from the assumed form of the motion equations. Statistical mechanics and kinetic theory provide an understanding of the correspondence between microscopic time averages and macroscopic continuum behavior.⁵ The catch in applying this correspondence is that any desired equation of state and transport information has to be obtained from carefully chosen simulations, with no guarantee that the number-dependence of the results is small or that the state dependence of the constitutive properties is simple. In simulations based on particle mechanics the main problems are (i) making a clever choice for the interparticle forces, (ii) developing appropriate boundary conditions to drive the flow, and (iii) finding useful means for analyzing the results of simulations. The force and boundary choices together with the analyses are useful to the extent that they help to interpret physical reality.

⁴Gleick, *Chaos* (1989).

⁵Hoover, *Computational Statistical Mechanics* (1991).

Continuum mechanics begins instead with *assumed* constitutive relations (nothing whatever needs to be said about particles or forcelaws). These continuum constitutive relations, combined with the conservation laws for mass, momentum, and energy, take the form of *partial* differential equations. These partial differential equations are enough to evolve the state of a continuum, including the fluxes of mass, momentum, and energy within it, from given initial conditions, subject to the imposed boundary conditions. In simulations based on continuum mechanics the main problems are (i) a clever choice of constitutive relations and (ii) a robust algorithm for solving the evolution equations subject to the imposed boundary conditions.

The two approaches, particle and continuum, can agree with one another provided that the continuum constitutive equations correspond to the assumed interparticle forces, and provided that the microscopic fluctuations which are absent in continuum mechanics can be ignored. We will see that the two approaches can also be related to one another through Smooth Particle Applied Mechanics, a method which uses *particles* to solve problems in *continuum* mechanics. Before proceeding with a description of SPAM let us first consider the fundamentals of classical particle mechanics and continuum mechanics.

1.3 Newton's Particle Mechanics

Particle mechanics is built on Isaac Newton's Laws, which linked together earlier intuitive ideas in a new and analytic way. Space and time were primitive notions, with roots predating history. Mass and force are newer concepts, required for the foundation which underlies the structure of scientific understanding. *Mass* is a convenient measure for quantities both rare, the "Troy ounce", and common, the "metric tonne". Navigation and the definition of spatial boundaries require the notion of *length*. Meetings, for business or for pleasure, require *time*.

Newton linked these ideas together by applying his discovery of calculus and differential equations. His resulting Second Law of motion,

$$F = m\ddot{r} = m\dot{v} = ma ,$$

links together the notions of mass, length, and time through the limiting

time rates of change ,

$$\frac{\Delta r}{\Delta t} \rightarrow \dot{r} = v ; \quad \frac{\Delta v}{\Delta t} \rightarrow \dot{v} = \ddot{r} = a ,$$

where the coordinate and velocity changes Δr and Δv occur during the infinitesimally-small time interval Δt . In this book we use superior single and double dots to indicate the first and second time “derivatives” in Newton’s calculus. In his Second Law of motion force is F , mass is m , velocity is v , and acceleration is a . The coordinate r is measured in a Cartesian system, with components $\{ x, y \}$ in two space dimensions and $\{ x, y, z \}$ in three.

Solving Newton’s motion equation where F is a constant vector (as in the frictionless motion of a mass point, or a nonspinning cannon ball, in a constant vertical gravitational field g) gives a parabolic trajectory :

$$a(t) = \dot{v}(t) = \ddot{r}(t) = F/m = g ;$$

$$v(t) = \dot{r}(t) = v(0) + gt ;$$

$$r(t) = r(0) + v(0)t + \frac{1}{2}gt^2 .$$

Notice that the two first-order (in time) ordinary differential equations require two initial conditions, $\{ r(0), v(0) \}$, for a unique solution to result.

Once the system considered becomes even a little more complicated—three bodies interacting with mutual inverse-square gravitational forces, for instance—where F_{ij} is the attractive force on mass m_i due to its “action at a distance” with mass m_j :

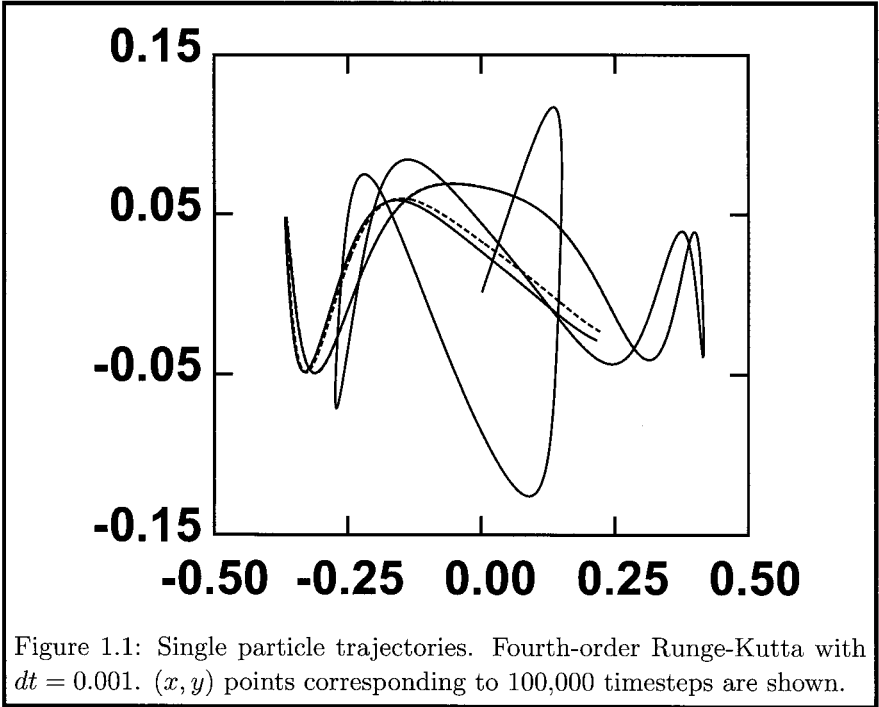
$$\{ F_{ij} = -Gm_i m_j (r_i - r_j) / |r_i - r_j|^3 \} ,$$

numerical methods are required to integrate the differential equations of motion.

Even a one-body problem, constrained by simple boundary forces, can have a relatively complicated “chaotic” (Lyapunov-unstable) solution, in which the growth of small errors is exponential in the time. See Sections 6.7 and 6.8 for a detailed approach to the exploration of Lyapunov instability. Analytic methods, based on truncated Taylor’s series, are quite hopeless for such problems. Consider, for instance, a single particle with unit mass, placed at the (x, y) origin with $(\dot{x} = \dot{y} = 1)$. Assume that this particle

moves in the field of four fixed neighbors at $x = \pm\frac{1}{2}, y = \pm\sqrt{\frac{3}{4}}$ where the forces affecting the motion are derived from the short-ranged pair potential,

$$\phi(r < 1) = 100(1 - r^2)^4 \longrightarrow F(r < 1) = 800r(1 - r^2)^3 .$$



The full curve in Figure 1.1 shows the resulting motion. In the broken-line rendering the initial conditions are only slightly different :

$$\dot{x} \rightarrow \dot{x} + 10^{-5} ; \dot{y} \rightarrow \dot{y} - 10^{-5} .$$

Figure 1.2, based on these same data, shows the *exponential* (Lyapunov unstable) growth of the deviation between these two trajectories.

The most useful numerical approach to solving such mechanics problems is the fourth-order Runge-Kutta integration used to generate the figures. The basic method is transparent as well as “self-starting”. That is, given the current values, the algorithm advances the evolving trajectory by a specified time interval dt . This fourth-order method has single-step errors

of order $dt^5/5!$ for a timestep dt . This integration technique, developed by Carl Runge from Martin Kutta's root-finding technique, estimates the changes of the dependent variables $\{ r, v \}$ from the known values $r(t)$ and $v(t)$ at time t to the desired values $r(t + dt)$ and $v(t + dt)$ at time $t + dt$ as the weighted averages of four time derivatives. A simpler but less-accurate second-order Runge-Kutta approach advances the coordinates and velocities through a timestep dt in two distinct stages, rather than four :

$$\{ \tilde{r}(t + dt) = r(t) + v(t)dt ; \tilde{v}(t + dt) = v(t) + a(t)dt \} .$$

$$\{ r(t+dt) = r(t) + \frac{dt}{2}[v(t) + \tilde{v}(t+dt)] ; v(t+dt) = v(t) + \frac{dt}{2}[a(t) + \tilde{a}(t+dt)] \} .$$

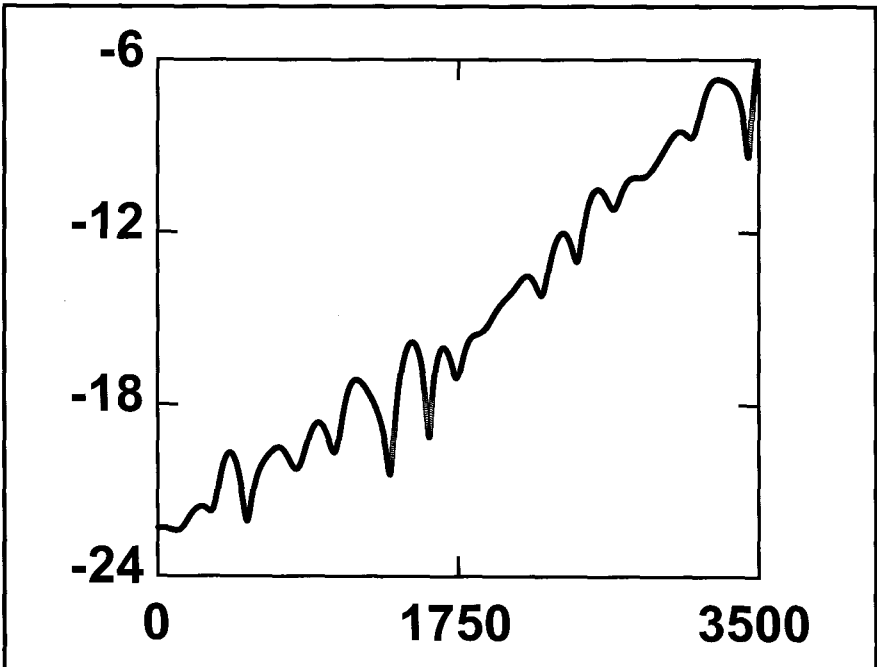


Figure 1.2: The natural logarithm of the squared phase-space deviation, $\Delta^2 \equiv \Delta p^2 + \Delta r^2$, between the two trajectories shown in Figure 1.1. The curve approximates a straightline relationship for 3500 timesteps. A straight line, on this semilogarithmic plot, corresponds to *exponential* (“Lyapunov unstable”) growth of trajectory perturbations. $dt = 0.001$.

The first-guess accelerations $\{ \tilde{a}(t + dt) \}$ are evaluated from the corresponding first-guess set of coordinates $\{ \tilde{r}(t + dt) \}$. The accuracy of this two-stage integration scheme is “second-order” in the timestep dt . This means that the coordinate and velocity errors incurred are of order dt^3 at each timestep. As a consequence, the error over a sufficiently-short, but fixed, time interval varies as dt^2 .

The better choice (more accurate, but still easy to program), justly popular after its hundred-year history of successes, is the classic four-stage fourth-order Runge-Kutta scheme :

$$\{ r(t + dt) = r(t) + \frac{dt}{6} [v(t) + 2\tilde{v}_2(t + \frac{dt}{2}) + 2\tilde{v}_3(t + \frac{dt}{2}) + \tilde{v}_4(t + dt)] \} ;$$

$$\{ v(t + dt) = v(t) + \frac{dt}{6} [a(t) + 2\tilde{a}_2(t + \frac{dt}{2}) + 2\tilde{a}_3(t + \frac{dt}{2}) + \tilde{a}_4(t + dt)] \} .$$

The new coordinates and velocities at time $t + dt$ are accurate through terms of order dt^4 . The intermediate coordinates and velocities $\{ \tilde{r}_i, \tilde{v}_i \}$ are given by the time derivatives evaluated in three successive stages, from $\{ \tilde{r}_2, \tilde{v}_2; \tilde{r}_3, \tilde{v}_3; \tilde{r}_4, \tilde{v}_4 \}$, after the initial evaluation of $\{ \dot{r}_1(t), \dot{v}_1(t) \}$ from $\{ r_1, v_1 \} = \{ r(t), v(t) \}$:

$$\{ \tilde{r}_2(t + \frac{dt}{2}) = r(t) + \frac{dt}{2} v_1(t) \} ; \{ \tilde{v}_2(t + \frac{dt}{2}) = v(t) + \frac{dt}{2} a_1(t) \} ;$$

$$\{ \tilde{r}_3(t + \frac{dt}{2}) = r(t) + \frac{dt}{2} \tilde{v}_2(t + \frac{dt}{2}) \} ; \{ \tilde{v}_3(t + \frac{dt}{2}) = v(t) + \frac{dt}{2} \tilde{a}_2(t + \frac{dt}{2}) \} ;$$

$$\{ \tilde{r}_4(t + dt) = r(t) + dt \tilde{v}_3(t + \frac{dt}{2}) \} ; \{ \tilde{v}_4(t + dt) = v(t) + dt \tilde{a}_3(t + \frac{dt}{2}) \} .$$

The coordinates and velocities at each of the latter three stages follow from the velocities and coordinates computed in the previous stage. The last set of intermediate coordinates and velocities, $\{ \tilde{r}_4, \tilde{v}_4 \}$, are required for the final fourth-order derivatives.

Finally the derivatives at the four stages ,

$$\{ \dot{r}_1(t), \dot{v}_1(t); \dot{r}_2(t + \frac{dt}{2}), \dot{v}_2(t + \frac{dt}{2}); \dot{r}_3(t + \frac{dt}{2}), \dot{v}_3(t + \frac{dt}{2}); \dot{r}_4(t + dt), \dot{v}_4(t + dt) \} ,$$

are averaged, with weights $\{ 1/6, 1/3, 1/3, 1/6 \}$, to advance $\{ r(t), v(t) \}$ to $\{ r(t + dt), v(t + dt) \}$. Such multistage Runge-Kutta algorithms are most easily programmed by storing all of the dependent variables ($\{ r, v \}$ in this case) in a vector (of length $4N$ for N particles in two-dimensional space and $6N$ for N particles in three-dimensional space). Their computed time derivatives $\{ \dot{r}, \dot{v} \}$ are stored in a second vector of the same length. For more details see Section 4.4.

A system composed of Newtonian particles requires a definite number of “degrees of freedom” (independent coordinates) for a complete description of its “configuration” in space. For point masses the number of degrees of freedom is the dimensionality multiplied by the number of particles. For rigid bodies additional *rotational* degrees of freedom (angles) are required, one of them in two dimensions and two in three dimensions. Because computer storage is relatively cheap, the number of degrees of freedom which can be followed numerically depends primarily on computer processor speeds and the number of processors. Machines with *millions* of processors are now on the drawing boards.⁶

Today Runge-Kutta integration makes it possible to follow the motion of *billions* of mutually interacting particles for as many as a *million* timesteps. This is the limit of what can be done today. The timestep dt cannot be too large. It is limited by the time required for adjacent particles to exchange information at the speed of sound. If the particles are microscopic models of atoms then the total simulated time is pitifully small, no more than a microsecond of real time, and there is no prospect whatever for reaching times of even one second for macroscopic amounts of matter. The physical extent of such an atomistic model is likewise very limited. It can be no more than a cubic micron. By contrast, the original Gingold-Lucy-Monaghan applications of smooth particles were *astrophysical*, with interstellar particle length scales and correspondingly long times. Today—and even in the foreseeable future—it is absolutely necessary to consider a “continuum” description of matter to simulate and discuss interesting and challenging scientific problems on the length and time scales relevant to men.

1.4 Eulerian and Lagrangian Continuum Mechanics

Matter distributed continuously in space, with a mass density ρ depending upon location $\rho(r)$, can require an *infinite* number of degrees of freedom for its description. But so long as the material properties vary smoothly in space it is possible to develop *exact* differential equations governing the properties’ time evolution. Consider a one-dimensional flow in which the density $\rho(x, t)$ and velocity $v_x(x, t)$ vary continuously and differentiably in space and time (so that the spatial derivatives $\partial\rho/\partial x$ and $\partial v_x/\partial x$ are also well-defined continuous functions in space and time). Focus on a sufficiently small element of length dx , fixed in space. During a short time

⁶R. Preston, New Yorker Magazine, 11 April 2005.

interval dt the net change of mass within dx can then be expressed as the difference of the (ρv_x) flows in and out at the element's two endpoints ,

$$[(\rho v_x)_{x-(dx/2)} - (\rho v_x)_{x+(dx/2)}]dt .$$

With the length dx fixed, the change of mass with time can be simplified :

$$\frac{\partial(\rho dx)}{\partial t} \equiv dx \frac{\partial \rho}{\partial t} = (\rho v_x)_{x-(dx/2)} - (\rho v_x)_{x+(dx/2)} .$$

In the limit that both the time interval dt and the element length dx are sufficiently small, this statement of mass conservation gives an *exact* partial differential equation (the continuity equation) for the changing mass density at a fixed location :

$$\frac{\partial \rho}{\partial t} = -\frac{\partial(\rho v_x)}{\partial x} = -\nabla_x \cdot (\rho v_x) .$$

In three space dimensions, where the flow velocity is the vector $v = (v_x, v_y, v_z)$, the continuity equation has exactly this same form :

$$\frac{\partial \rho}{\partial t} = -\nabla \cdot (\rho v) = -\nabla_x(\rho v)_x - \nabla_y(\rho v)_y - \nabla_z(\rho v)_z .$$

Again the *partial* derivative $\partial\rho/\partial t$ indicates the change of density at a fixed point in space.

An alternative description, using the “comoving” time derivative, the derivative following the motion, $d/dt \equiv \cdot$ (a “superior dot”), can be evaluated from the evolution of two nearby points, embedded in the material and initially separated by dx . For simplicity, consider the evolution of the two neighboring points in one dimension $\{x_0 \pm \frac{dx}{2}\}$ for a small time interval dt and a sufficiently small moving element of length dx :

$$\{ x_0 \pm \frac{dx}{2} \} \longrightarrow \{ x_0 \pm \frac{dx}{2} + v_0 dt \pm \frac{dx}{2} (\partial v / \partial x)_t dt \} .$$

Evidently the initial separation of the points $dx(t_0) \equiv x_{\text{right}} - x_{\text{left}}$ changes whenever there is a velocity gradient. To first order in dt the change is $(\partial v / \partial x)_t dx dt$ during the time dt :

$$x_{\text{right}}(t_0) \rightarrow x_{\text{right}}(t_0) + v dt + \frac{dx}{2} (\partial v / \partial x)_t dt ;$$

$$x_{\text{left}}(t_0) \rightarrow x_{\text{left}}(t_0) + v dt - \frac{dx}{2} (\partial v / \partial x)_t dt ;$$

$$dx(t_0) \rightarrow dx(t_0)[1 + (\partial v / \partial x)_t dt] = dx(t_0 + dt) ;$$

$$\frac{[dx(t_0 + dt) - dx(t_0)]}{dt dx(t_0)} \rightarrow \frac{d \ln dx}{dt} \equiv -\frac{d \ln \rho}{dt} = \frac{\partial v_x}{\partial x} .$$

In two or three dimensions the corresponding *comoving* version of the continuity equation is as follows :

$$\frac{d\rho}{dt} = \dot{\rho} = -\rho \nabla \cdot v \longleftrightarrow \frac{d \ln \rho}{dt} = -\nabla \cdot v .$$

The continuity equation is a fundamental representation of mass conservation, equating the mass change to differences of mass flow.

The change and flow of momentum within a small moving volume element is calculated in a similar way, except that an additional momentum flux, due to “action at a distance” (from forces) adds the *comoving* momentum flux $P \equiv -\sigma$ to the convective flux $\rho v v$:

$$\frac{\partial(\rho v)}{\partial t} = -\nabla \cdot (P + \rho v v) \equiv \nabla \cdot (\sigma - \rho v v) .$$

This “motion equation”, which gives the evolution of v and hence—by integration—the evolution of the system’s configuration $\{ r \}$, is a fundamental representation of momentum conservation. Just as in deriving the continuity equation, the equation of motion results from equating an overall change to a difference of corresponding flows. P is the pressure tensor, the negative of the stress tensor σ , $P \equiv -\sigma$. P is a momentum flux. P_{xy} , for instance, the xy component of P , is the comoving flow of x momentum in the y direction.

It is usual to term the evolution equations at a *fixed* point in space the “Eulerian” evolution equations. For the continuity equation and equation of motion the Eulerian forms are :

$$\frac{\partial \rho}{\partial t} = -\nabla \cdot (\rho v) ; \quad \frac{\partial(\rho v)}{\partial t} = -\nabla \cdot (P + \rho v v) .$$

The equivalent *comoving* evolution equations are termed “Lagrangian”. Lagrangian time derivatives are defined for coordinates which follow the motion. The Lagrangian continuity and motion equations are :

$$\dot{\rho} = -\rho \nabla \cdot v ; \quad \dot{v} = -[\nabla \cdot P]/\rho = [\nabla \cdot \sigma]/\rho .$$

Either the Eulerian or the Lagrangian equations can serve as the basis of numerical simulation techniques.

In addition to the flow of mass, as described by the “continuity equation”, and the flow of momentum, as described by the “equation of motion”, continuum mechanics also accounts for the flow of energy, a third conserved

quantity. Just as in the case of momentum flux, experience shows that the flow of energy can include both “convective” and “conductive” effects. Convection is bodily transport (as is plainly visible in moving clouds or flames) which takes place at the local fluid velocity v . Conduction is that *additional* transport which still occurs in the absence of fluid motion (or, equivalently, transport occurring in the coordinate frame *comoving* with the fluid). The transmission of heat in a motionless solid rod is the simplest example of co-moving energy conduction. Momentum is likewise transmitted through the mechanism of forces (action at a distance) as is described by the pressure tensor. The distinction between free-streaming convective transport and collisional conductive transport is obvious and natural in particle mechanics. The same distinction requires new, and less obvious, phenomenological relations in continuum mechanics. On a macroscopic continuum level the stress tensor $\sigma = -P$ [momentum flow per unit area and time] and heat flux vector Q [energy flow per unit area and time] replace microscopic interparticle forces as the underlying *ad hoc* nonconvective mechanisms for transporting momentum and energy.

From the classical point of view of particle mechanics it is natural to separate the total energy E into two parts, potential and kinetic, $E = \Phi + K$. In the simplest case, a Cartesian-coordinate description of mutually interacting points, the potential energy depends solely on the coordinates and the kinetic energy depends solely on the velocities. For isolated systems the total energy E is fixed. Consider, as a simple example, a single harmonic oscillator, with coordinate q , momentum $p = m\dot{q}$, and force constant κ :

$$E = \phi + K ; \phi = \frac{\kappa q^2}{2} ; K = \frac{p^2}{2m} = \frac{m\dot{q}^2}{2} .$$

From a given initial condition the state vector (q, p) evolves on the constant-energy ellipse, $E(q, p) = E(t = 0)$. In continuum mechanics the system’s total energy density—energy per unit volume, with units [mass][length] $^{2-D}$ [time] $^{-2}$ in D space dimensions—is likewise separated into two parts ,

$$\rho e_{\text{total}} = \rho e + (\rho v^2/2) ,$$

where e is the “internal energy” per unit mass. It is important to recognize that the internal energy of continuum mechanics includes not only the microscopic particle potential energy, but also that part of the particles’ kinetic energy which corresponds to macroscopic “heat” energy. The kinetic energy density associated with macroscopic motion, $\frac{\rho v^2}{2}$, or the corre-

sponding contribution from rotation, makes no contribution to the “internal energy” per unit mass e .

Like the changes of kinetic and potential energy, the macroscopic concepts of heat and work refer to energy changes associated with microscopic motion (“heat”) and with macroscopic motion (“work”) with the latter energy change resulting from the time-variation of macroscopic coordinate variables. The First Law of Thermodynamics is usually written as a straightforward energy balance, in which the change of total system energy, dE , has two parts, the heat absorbed from the surroundings, dQ , and the work done on those surroundings, dW . If the various changes occur within a short time dt , and can still be separated into thermal and mechanical parts, then the First Law of Thermodynamics can be written as a differential equation :

$$dE = dQ - dW \longleftrightarrow \dot{e} = (\dot{E}/m) = (\dot{Q}/m) - (\dot{W}/m) .$$

The latter expression can also be applied locally, where the energy per unit mass $e = E/m$ is a *field* variable, defined at all points within the system. The energy changes $\dot{Q}dt$ and $\dot{W}dt$ due to heat absorbed and work done are both considered in the *comoving* frame which moves with the system’s local velocity. The differential form of the First Law separates energy changes (in this comoving frame) into conductive changes (“heat”) and energy changes associated with coordinates (“work”). Work can include deformation as well as motion within an external field. This separation of energy changes into heat and work is required for a thermodynamic description.

Mechanics introduces the notion of pressure as the force driving volume changes. *Thermodynamics* introduces a second notion, temperature, as the driving mechanism for conductive energy changes, the flow of heat. The *microscopic* analogs of these macroscopic concepts invariably involve averaging, usually over a large number of particles and a long time.⁵ Temperature, for instance, is most simply defined as the mean (microscopic) kinetic energy per Cartesian degree of freedom (when measured in the “comoving” coordinate frame which moves at the material velocity v) :

$$DkT/2 \equiv \langle m(v_{\text{micro}} - v)^2/2 \rangle ,$$

in D space dimensions, where k is Boltzmann’s constant. A more general development introduces the ideal-gas thermometer based on this definition, with the thermodynamic temperature T characterizing any system (even

⁵Hoover, *Computational Statistical Mechanics* (1991).

a quantum system) with which the (classical) thermometer is in thermal equilibrium.

1.5 Computer Simulation of Microscopic Particle Motion

Molecular dynamics, simulating the evolution of microscopic particle trajectories with computers, has been an active research field for over half a century. The early simulations, at Brookhaven,⁷ Livermore,⁸ and Los Alamos,⁹ were mostly devoted to solving Newton's equations of motion ,

$$\left\{ \ddot{r} = \dot{v} = \frac{F}{m} \right\} ,$$

where the force F on each particle is the vector sum of contributions from its nearby neighbors. These Newtonian motion equations apply to isolated systems for which the total system energy is a constant of the motion.

Vineyard's studies of radiation damage in solids were an exception to this rule. He introduced special dissipative viscous boundary forces ,

$$\left\{ \frac{F_{\text{viscous}}}{m} \equiv -\frac{v}{\tau} \right\} ,$$

designed to reduce the influence of boundaries on interior dynamics. The parameter τ was chosen to optimize the damping of internally-generated sound waves incident on the system boundary.

Much of the early activity in molecular dynamics was devoted to evaluating the thermal and mechanical equations of state for given potential energy functions :

$$\Phi \longrightarrow E(V, T) , P(V, T) .$$

Temperature was evaluated by using the ideal-gas-thermometer definition:

$$\langle p_x^2 = p_y^2 = p_z^2 \rangle \equiv mkT ; p = mv ,$$

for particles of mass m in thermal equilibrium with an ideal gas thermometer maintained at a temperature T . Here k is Boltzmann's constant.

Pressure was evaluated by measuring the mean momentum flux, which separates into kinetic and potential contributions. For a system with

⁷Vineyard, with Gibson, Goland, and Milgram (1960).

⁸Alder and Wainwright (1958).

⁹Fermi, Pasta, and Ulam, as described by Tuck and Menzel (1972).

pairwise-additive forces ,

$$\Phi = \sum_{i < j} \phi_{ij} \longrightarrow F_i = \sum_j F_{ij}(r_{ij}) ; r_{ij} \equiv r_i - r_j ; \{ i, j \} \subset V ,$$

the instantaneous pressure tensor P , the local average of momentum flux in a comoving volume V , has the form :

$$PV = \sum_i \frac{p_i p_i}{m} + \sum_{i < j} r_{ij} F_{ij} ; r_{ij} = r_i - r_j ; F_{ij} = -\nabla_i \phi_{ij} .$$

To clarify the meaning of our shorthand notation let us write out the four components $\{ P_{xx}, P_{xy}, P_{yx}, P_{yy} \}$ of the pressure tensor in two space dimensions :

$$P_{xx}V = \sum_i (p_x^2/m)_i + \sum_{i < j} (x^2 F/r)_{ij} ;$$

$$P_{xy}V = \sum_i (p_x p_y/m)_i + \sum_{i < j} (xy F/r)_{ij} = P_{yx}V ;$$

$$P_{yy}V = \sum_i (p_y^2/m)_i + \sum_{i < j} (y^2 F/r)_{ij} ;$$

with the definitions of the pair quantities :

$$x_{ij} = x_i - x_j ; y_{ij} = y_i - y_j ; r_{ij} = \sqrt{x_{ij}^2 + y_{ij}^2} ; F_{ij} = F(r_{ij}) .$$

The tensor components of P describe the flux (flow per unit area and time) of momentum in space, so that P_{xy} describes the flow of x momentum in the y direction. Rotational stability requires that P be symmetric, $P_{xy} = P_{yx}$, not just for pairwise-additive systems, but in general.⁵

Approximately 25 years were required to complete this phase of the development of molecular dynamics. It is now routine to generate accurate thermodynamic properties for classical systems with given interparticle forces. Work has continued, mostly on more elaborate models for polyatomic molecules, but such activities are hampered by difficulties in forcing quantum systems (“real matter”) to be described by a classical model.

During the last 25 years methods based on molecular dynamics have been developed for treating the nonequilibrium problems more closely related to the subject of this book.¹⁰ On the particle level there is no problem

⁵See page 189 of my *Computational Statistical Mechanics* (1991).

¹⁰Hoover (1997).

in formulating the flows of momentum and energy (the pressure tensor P and the heat flux vector Q). The microscopic expressions for these fluxes have no special nonequilibrium parts. They have exactly the same forms at equilibrium as they do away from equilibrium. The main difficulties in simulating nonequilibrium microscopic systems are (i) formulating proper boundary conditions to drive the flows away from equilibrium and (ii) absorbing the heat these flows generate. Feedback and control are the familiar concepts engineers would use and implement in order to deal with these latter needs.

Shuichi Nosé formalized and implemented the key new idea required for *control* in molecular dynamics: *thermostat forces* designed to enforce a specified *time-averaged* ideal-gas temperature on particular degrees of freedom.¹¹ He and Hans Andersen and I also formulated *barostat forces* designed to enforce a particular average pressure (by making the corresponding volume a function of time). Nosé’s ideas were a direct outgrowth of Gibbs’ statistical mechanical approach to equilibrium averages, but have the distinct advantage of being equally applicable to nonequilibrium systems. Nosé’s ideas make it possible to simulate stationary shear flows and heat flows, giving direct measurements of shear viscosity and thermal conductivity, even far from equilibrium. The consequences of his thermostat forces for the development of statistical mechanics are discussed in the next Section.

1.6 Liouville’s Theorem; Statistical Mechanics

Liouville’s Theorem provides an interesting link between Nosé’s mechanics and the old (1883) Gibbs-Boltzmann equilibrium statistical mechanics.¹² Liouville’s Theorem is a fundamental building block for equilibrium statistical mechanics. It describes the flow of the probability density $f(q, p, t)$ in the “phase space” composed of all the particle coordinates and momenta, $\{q, p\}$. The underlying (q, p) flow is governed by the “Hamiltonian” \mathcal{H} :

$$\mathcal{H} = K(p) + \Phi(q) \rightarrow \left\{ \dot{q} = +\frac{\partial \mathcal{H}}{\partial p} ; \dot{p} = -\frac{\partial \mathcal{H}}{\partial q} \right\} .$$

The Theorem is a direct consequence of Hamiltonian mechanics. It

¹¹Nosé (1991).

¹²Hoover, Journal of Chemical Physics (1998).

establishes that the time derivative of f , following the motion, vanishes :

$$\begin{aligned} \left(\frac{\partial f}{\partial t}\right) &= -\sum \frac{\partial(f\dot{q})}{\partial q} - \sum \frac{\partial(f\dot{p})}{\partial p} \rightarrow \\ \dot{f} = df/dt &= \left(\frac{\partial f}{\partial t}\right) + \sum \dot{q} \cdot \nabla_q f + \sum \dot{p} \cdot \nabla_p f = \\ -f \sum \left(\frac{\partial \dot{q}}{\partial q} + \frac{\partial \dot{p}}{\partial p}\right) &= -f \sum \left(\frac{\partial^2 \mathcal{H}}{\partial q \partial p}\right) + f \sum \left(\frac{\partial^2 \mathcal{H}}{\partial p \partial q}\right) \equiv 0, \end{aligned}$$

where the sums include all the degrees of freedom required to describe the system's "phase" (q, p) . Evidently it is an exact consequence of Hamiltonian mechanics that *equilibrium* systems, for which $\partial f/\partial t$ must vanish also, correspond to phase space distributions in which $f(q, p)$ is exactly the same for all accessible states :

$$\dot{f} = 0 \rightarrow \left(\frac{\partial f}{\partial t}\right)_{\text{eq}} \equiv 0.$$

Nosé's *thermostated* systems, described with thermostat forces, can also be discussed from the standpoint of Liouville's Theorem, modified to include the frictional contributions of the nonHamiltonian "Nosé-Hoover" thermostat forces $\{-\zeta p\}$:

$$F = -\nabla\Phi - \zeta p \rightarrow -f \frac{\partial \dot{p}}{\partial p} = f\zeta \rightarrow$$

$$\dot{f} = 0 \xrightarrow{\zeta} \dot{f}/f = \sum_{\{p\}} \zeta = \dot{S}/k = -\sum_{\{T\}} \dot{Q}/kT.$$

The "friction coefficient" ζ obeys a feedback equation based on the ratio of the current kinetic energy K to the desired average K_0 , with both represented as sums over all the thermostated degrees of freedom :

$$\dot{\zeta} = \left[\left(\sum \frac{p^2}{m} / \sum kT_0 \right) - 1 \right] / \tau^2.$$

Here τ is a phenomenological relaxation time describing the response of the Nosé-Hoover thermostat with temperature T_0 corresponding to the kinetic energy K_0 . See Reference [5] for more details and many worked-out examples.

With Nosé's friction included, the comoving phase-space density f *changes* according to \dot{S} , the external entropy production rate due to transfers of heat from the reservoirs at $\{ T \}$, at the rates $\{ \dot{Q} \}$, to the system. These are the rates at which heat is transferred from Nosé's reservoirs divided by the corresponding reservoir temperatures. In nonequilibrium steady states heat flows from the system to the reservoirs, on average, so that $\langle \dot{Q}/T \rangle$ is negative, and the external entropy increases. The transferred heat increases the states available to the reservoirs while correspondingly decreasing the states available to the nonequilibrium system interacting with those reservoirs.

Entropy had already been associated with phase-space states by Gibbs¹³ and Boltzmann¹⁴ by 1883. Both men recognized the probabilistic tendency of chaotic mechanical systems to explore as many such states as possible and characterized the "approach to equilibrium" in terms of a natural increase in the number of available states. For over a century nonequilibrium systems have been viewed as approaching equilibrium through an increase in the number of available states. Nosé's approach leads instead to a new understanding of nonequilibrium systems in terms of the intrinsic *rarity* of their states. In Nosé's mechanics the overall increase in available states occurs only within the external heat reservoirs where the nonequilibrium system deposits its generated heat. The nonequilibrium system coupled to these reservoirs has itself *fewer and fewer* states available as time goes by. Nosé's feedback constraint forces restrict the system dynamics into an ever-smaller fractional-dimensional region of phase space.

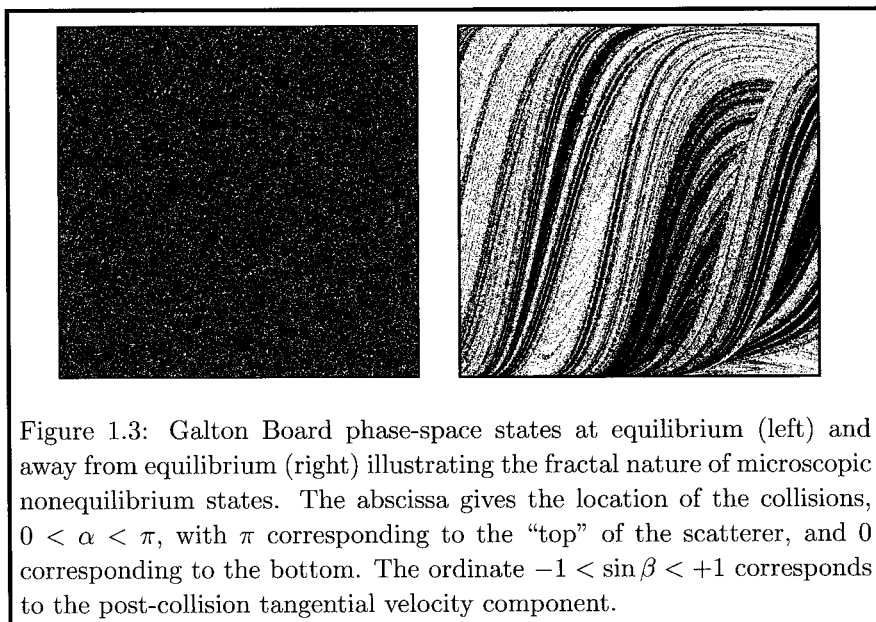
Thus external entropy production—*gain*—corresponds to internal entropy *loss*, with the system's phase-space density shrinking onto a nonequilibrium "attractor" of ever smaller volume. Because the external entropy production for nonequilibrium stationary states is necessarily positive, the internal phase-space probability density f grows exponentially with time as its phase-space extent shrinks. The nonequilibrium phase-space distribution function $f(q, p, \zeta, t)$ eventually *diverges* in any steady state so that the corresponding phase volume described by the stationary state actually *vanishes*. The new dynamical approach developed by using Nosé's mechanics to simulate nonequilibrium steady states shows very directly that such nonequilibrium states are extremely rare in the sense that they occupy a "multifractal" (fractional-dimensional) vanishing volume of phase space.

Figure 1.3 illustrates this nonequilibrium volume and dimensionality

¹³Gibbs (1902).

¹⁴Boltzmann, as described by Cercignani (1998).

reduction for the simplest possible system, the “Galton Board”, in which a single particle is accelerated by gravity while moving within a lattice of fixed scatterers.¹⁵ The ensuing chaotic motion is constrained to occur at constant speed [which is equivalent to a constant kinetic temperature proportional to $(p_x^2 + p_y^2)/mk$]. This constant-speed motion generates a (time-averaged) stationary nonequilibrium state. The (time-averaged) net effect of the motion is to transfer gravitational field energy to a heat reservoir through the medium of the moving particle. This energy transfer, corresponding to a heat loss, substantially reduces the states available to the moving thermostated particle, as is shown in Figure 1.3 .



The Figure shows the available phase-space states, both at and away from equilibrium, for the collisions of a single thermostated hard disk moving through an infinite periodic triangular lattice of fixed disks. In both cases the motion occurs at constant kinetic energy either with or without a vertical external accelerating field. With the field *off* (equilibrium) all the states in the rectangular phase-space section shown in the Figure are

¹⁵Moran, Hoover, and Bestiale (1987).

equally likely. With the field *on* (nonequilibrium steady state) the distribution becomes a zero-volume “fractal” singular distribution. Various fractional dimensionalities have been defined and can be evaluated for relatively simple problems like this one. The “information dimension” of the attractor based on $\langle f \ln f \rangle$ is 1.8, while the “correlation dimension” based on $\langle f^2 \ln f \rangle$, is 1.6. There is a vast literature on this Galton Board problem.

1.7 Simulating Continua with Particles

Continuum mechanics is a “field theory” in which the various field variables $(\rho, v, \sigma, Q, \dots) = (\text{density, velocity, stress, heat flux, } \dots)$ vary continuously in both space and time. Because in principle continua involve an infinite number of degrees of freedom, it is necessary in practical computations somehow to truncate the description to a manageable finite number.

In some cases the field variables can be usefully expressed as truncated Fourier series. Another approach to making the simulation work manageable is to use the “finite-element method”. That method visualizes the continuum as partitioned into a set of contiguous space-filling “finite elements”, each described by a finite number of degrees of freedom. The field variables within a particular element then vary according to an appropriate “shape function”. A linear representation is the simplest. Suppose that the continuum variable $C(x)$ has specified values at the two endpoints of an interval of length dx centered at x . In one dimension the *linear* interpolation of $C(x) = a + bx$ between the two known values at the ends of the interval requires just the two constants (a, b) :

$$C_- = C(x - \frac{dx}{2}) \text{ and } C_+ = C(x + \frac{dx}{2}) \longrightarrow a = \frac{C_- + C_+}{2} - bx ; b = \frac{C_+ - C_-}{dx} .$$

A similar linear interpolation function can be developed in two dimensions ($a + bx + cy$ for triangular elements) or in three dimensions ($a + bx + cy + dz$ for tetrahedral elements). This is a natural approach to follow in a Lagrangian simulation, in which the elements follow the motion of the continuum. If the variation of a continuum property $C(x, y)$ within a two-dimensional element has the “bilinear” shape function, $a + bx + cy$, it is evident that the shape functions for any two contiguous triangles must agree along their common linear boundary. On the other hand, with this bilinear approach, the *gradient* of C *perpendicular* to such a common boundary is typically discontinuous. Continuous spatial derivatives would require at least quadratic shape functions.

“Finite difference methods” are another possibility. These are best suited to Eulerian calculations for which a fixed Cartesian grid made up of line segments of equally-space points, or of squares in two dimensions, or cubes in three, is the simplest choice. Replacing the spatial derivatives $\{ \nabla \cdot v, \nabla \cdot P, \nabla \cdot Q \}$ on the righthandsides of the continuum equations by appropriate differences (based on Taylor’s series) then gives rise to a finite set of ordinary differential equations for the time development of the nodal values.

Consider a regular one-dimensional grid of points separated by line segments of length dx , with each line-segment endpoint characterized by its own temperature T . Recall that the phenomenological equation for heat transfer in one dimension is the Fick-Fourier law :

$$\frac{\partial T}{\partial t} = D_T \frac{\partial^2 T}{\partial x^2} ,$$

where D_T is the “thermal diffusivity”, with units $[\text{length}]^2/[\text{time}]$. For the discrete fixed-grid-point model of a heat-conducting continuum, this *partial* differential heat-transfer equation is replaced by a finite-difference approximation to the spatial derivative, corresponding to the approximate set of *ordinary* differential equations :

$$\left\{ \dot{T}_i = \frac{D_T}{dx^2} [T_{i+1} - 2T_i + T_{i-1}] \right\} ,$$

for the grid-point temperatures’ evolution. The underlying assumption is that the second-difference representation of ∇^2 [with its accompanying error of order $(dx)^2 \nabla^4 T$] is adequate. More details and applications of the finite-difference approach are given in the next Chapter.

When material motion (“flow”) is included in the evolution it is usual to contrast Eulerian and Lagrangian techniques. The Eulerian approach uses a fixed grid. This approach has difficulty in tracking the motions of the *boundaries* of the various described materials. The Lagrangian approach makes use of a *comoving* grid (moving with the material velocity) so that material boundaries define, and coincide with, element boundaries.

The Lagrangian finite-element approach, with moving triangles or tetrahedra (or with more elaborate elements, such as shells or hexahedra) has difficulty in dealing with largescale irregular deformations. If the grid becomes badly distorted, with strains of order unity, so that the zones can become tangled, the whole formalism fails. This is because the finite-difference formulae, which properly describe the derivatives and surface normals needed for flux calculations, are only accurate for *small* deformations. They become

increasingly less accurate for large ones and eventually lead to instabilities. Figure 1.4 shows a Lagrangian mesh, composed of shell elements which deform in response to external shear and compressive forces.¹⁶

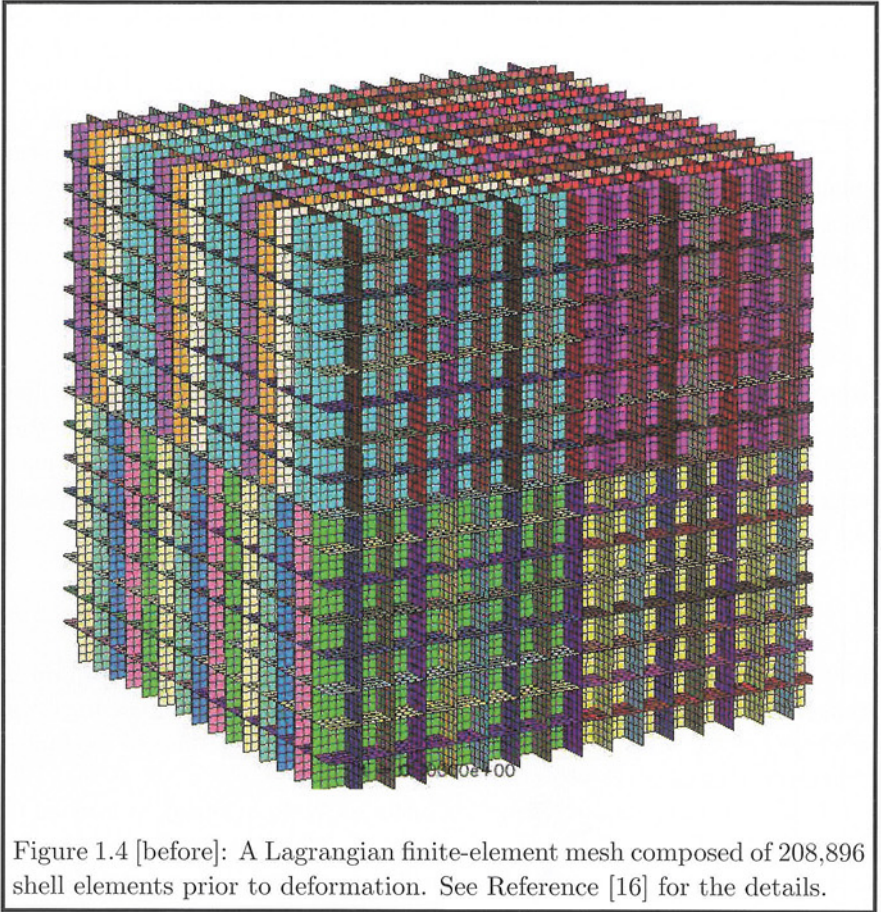


Figure 1.4 [before]: A Lagrangian finite-element mesh composed of 208,896 shell elements prior to deformation. See Reference [16] for the details.

A way to avoid the instability problems associated with Eulerian interface tracking and Lagrangian distortion and tangling is to compute derivatives of the continuum field variables on an *irregular* grid, where the grid is itself composed of sufficiently many moving particles. Though the use of an irregular grid to combat distortional instability seems paradoxical, the idea works because the “grid” of particles lacks a memory of its ini-

¹⁶Hoover and Hoover, (2005).

tial configuration, and is consequently self-healing. This particle-grid idea is included in the smooth-particle approach discovered jointly by Gingold, Lucy, and Monaghan. It is described in the next Section. Alternative approaches, which are computationally more cumbersome, consider *particles* moving within a regular Eulerian grid of field points. The “particle-in-cell” method is an example.¹⁷

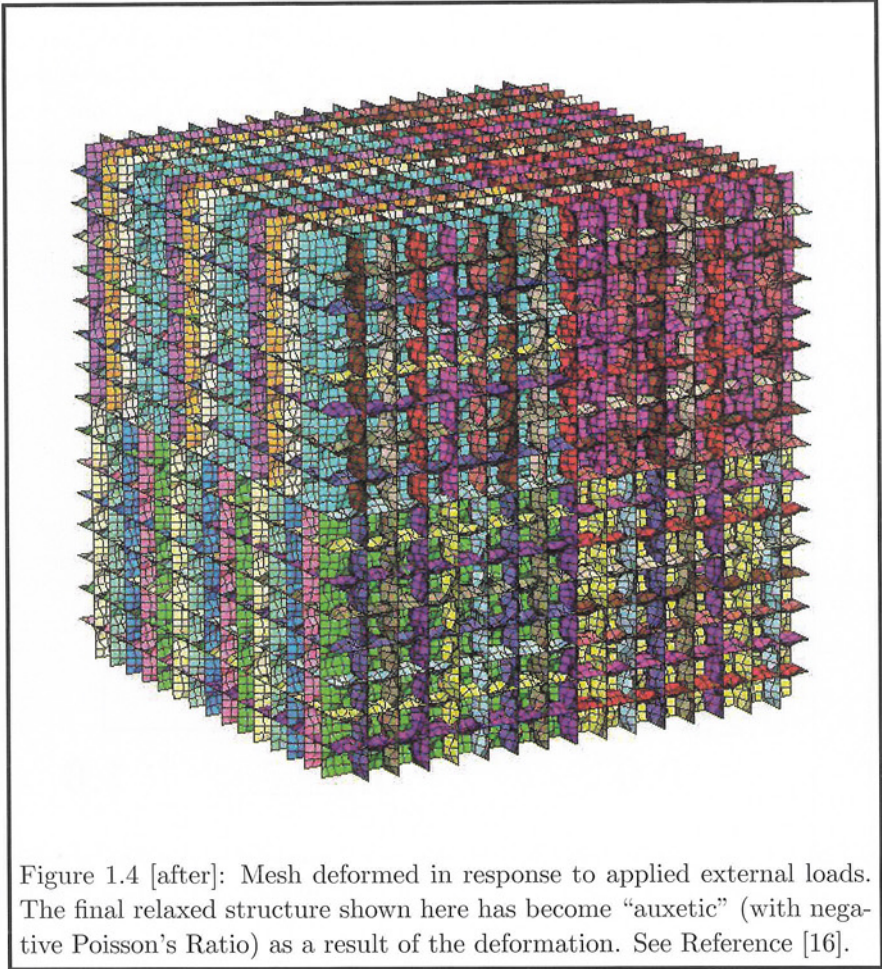


Figure 1.4 [after]: Mesh deformed in response to applied external loads. The final relaxed structure shown here has become “auxetic” (with negative Poisson’s Ratio) as a result of the deformation. See Reference [16].

¹⁷Birdsall and Langdon, *Plasma Physics via Computer Simulation* (1985).

1.8 SPAM [Smooth Particle Applied Mechanics]

SPAM began in 1976-1977 at Cambridge University's Institute of Astronomy. The discoverers were Robert Gingold, Leon Lucy, and Joseph Monaghan. At that time their research interests centered on complex astrophysical problems which were ill-suited to conventional Eulerian and Lagrangian simulation techniques. Their basic idea was, and is, to express all of the continuum variables on a grid composed of moving particles. If each particle is itself viewed as being distributed over space, with a normalized weight function w , then the mass density ρ at any point r in space can be defined as the sum of the densities $\{mw\}$ of all particles close enough to contribute:

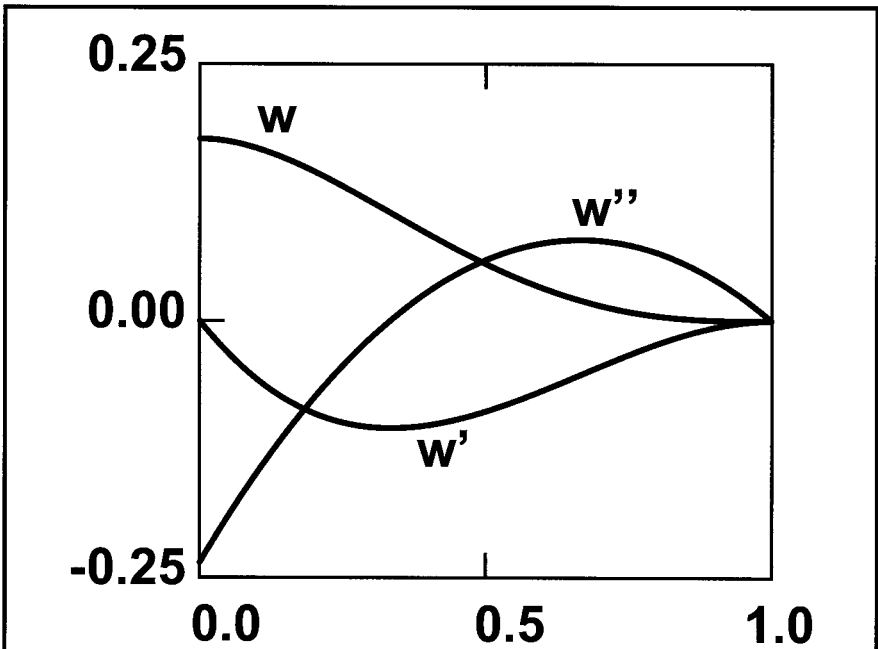


Figure 1.5: Lucy's weight function, along with its first and second derivatives, in two dimensions and with $h = 3$; the abscissa is (r/h) .

$$w(r < h) = \frac{5}{9\pi} \left[1 + \left(3\frac{r}{h} \right) \right] \left[1 - \left(\frac{r}{h} \right) \right]^3 .$$

This weight function gives the *simplest* possible smooth-particle recipes, with continuous first and second derivatives, as detailed in Chapter 3.

$$\rho(r) = \sum m_j w_{rj} ; w_{rj} = w(|r - r_j|) .$$

Lucy's weight function, which we use throughout this book to formulate and solve many of our example problems, is illustrated in Figure 1.5 .

Continuum properties associated with the particles can likewise be averaged to compute local values :

$$C(r) \equiv \sum m_j w_{rj} C_j / \sum m_j w_{rj} \rightarrow \rho(r) C(r) \equiv \sum m_j w_{rj} C_j .$$

This intuitive recipe for averages has particularly useful consequences for evaluating gradients, as we will see in detail in Chapter 3. Note particularly that only the weight function $w_{rj} = w(|r - r_j|)$ is affected by the gradient operator ∇_r :

$$\nabla_r(\rho C)_r \equiv \nabla_r \sum_j m_j w_{rj} C_j = \sum_j m_j C_j \nabla_r w_{rj} .$$

There is a significant difference between smooth-particle interpolation and the simpler Eulerian finite-difference and Lagrangian finite-element interpolation schemes. In the smooth-particle case the continuum variables associated with a particular particle, $\{ C_i \}$, typically *differ* from the field variables evaluated at the location of the particle, $\{ \langle C(r_i) \rangle \}$ because the latter averages include additional contributions from nearby particles. Gradients evaluated *at* the particles' locations $\{ \langle \nabla C \rangle(r_i) \}$ can then be used to evaluate the evolution of particle properties as solutions of ordinary differential equations $\{ \dot{C}_i \}$. Besides an elegant simplicity, this smooth-particle approach has the additional advantage that fracture and failure can be made to occur naturally and automatically. Even complex astrophysical problems can be treated with SPAM. A relatively recent example is the collision of a comet with the back side of Jupiter.¹⁸

I spell out and illustrate the remaining details of the numerical method in Chapter 3. Because the technique closely resembles molecular dynamics, but with more elaborate accelerations, we lay the groundwork here by sketching the molecular dynamics approach as it applies to a simple 16-particle example.

¹⁸Ahrens, Takata, O'Keefe, and Orton (1994).

1.9 Example: A Molecular Dynamics Simulation

To illustrate the simplest mass-point particle dynamics, “molecular dynamics”, consider a simple dynamical simulation. We begin with the 16 particles shown in the Figure 1.6 . The initial configuration is a square lattice. The initial velocities were first chosen at random from the square $(-1 < v_x, v_y < 1)$, and then modified to satisfy two constraints, (i) vanishing center-of-mass velocity :

$$\left(v_i \rightarrow v_i - \frac{1}{16} \sum v \right) \longrightarrow \sum v \equiv 0 ;$$

and (ii), a prescribed initial kinetic energy :

$$\left(v_i \rightarrow v_i \sqrt{32 / \sum v^2} \right) \longrightarrow \sum v^2 \equiv 32 .$$

The sums here include all 16 particles. The random number generator used to choose their initial velocities appears in Section 4.5 .

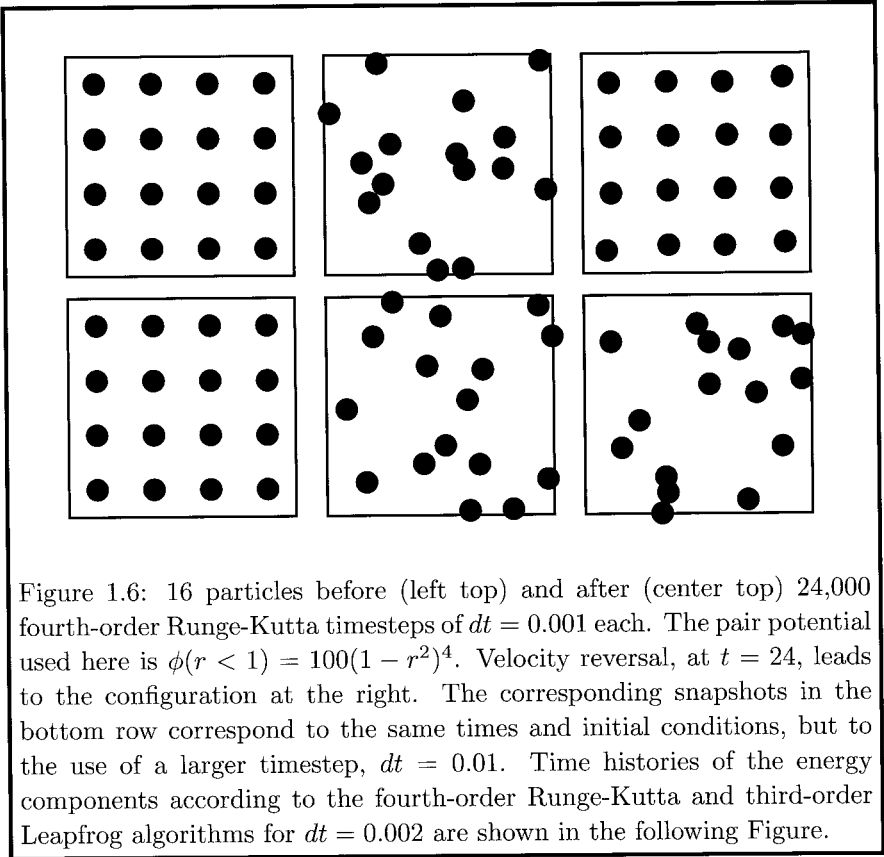
Two different integration algorithms were used to generate the configurations illustrated in Figure 1.6 . The fourth-order Runge-Kutta method used here was already detailed in Section 1.3 . The corresponding Fortran and C codes for this integrator are given in Section 4.4 . The simpler, but less accurate, “leapfrog” algorithm, also used here, is equivalent to a simple recipe for computing the coordinates at time $t + dt$ from two previously known coordinate values together with the current acceleration at time t . Rearrange the approximate expression for the acceleration ,

$$dt^2 a(t) \simeq r(t + dt) - 2r(t) + r(t - dt) ,$$

so as to *define* the new coordinate $r(t + dt)$ in terms of its predecessors at times t and $t - dt$:

$$r(t + dt) \equiv 2r(t) - r(t - dt) + dt^2 a(t) .$$

A comparison of the Taylor’s series expansion (in dt) for the two sides shows that the single-step error in the new coordinate is of order $\frac{1}{12} dt^4 \ddot{a}(t)$, so that the algorithm is “third-order”, accurate through terms of order $\dot{a} dt^3$.



With a particle mass of unity, $m = 1$, the initial kinetic energy of the system is $\sum mv^2/2 = 16$. For simplicity, let all pairs of particles interact with a simple short-ranged pair potential ϕ whenever the separation of the pair is less than unity :

$$\phi(r < 1) = 100(1 - r^2)^4 .$$

In the original configuration the total potential energy vanishes so that the total energy—a constant of the motion—is $E = K + \Phi = 16$.

Once the particles start to move, all interacting pairs with $r < 1$ will experience a repulsive force $F(r < 1) = -\nabla\phi$:

$$F(r < 1) = a(r) = 800r(1 - r^2)^3 .$$

We eliminate the need for special boundary forces by imposing *periodic* boundary conditions on the 4×4 box in which the motion takes place :

$$x < -2 \rightarrow x = x + 4 ; x > +2 \rightarrow x = x - 4 ;$$

$$y < -2 \rightarrow y = y + 4 ; y > +2 \rightarrow y = y - 4 .$$

In calculating the forces between Particle i and Particle j these same periodic boundaries require that the smallest (in absolute value) of the three possible separations, $r_{ij} = (x_{ij}, y_{ij})$, in both the x and the y directions :

$$x_{ij} = x_i - x_j \pm L \text{ or } x_{ij} = x_i - x_j ;$$

$$y_{ij} = y_i - y_j \pm L \text{ or } y_{ij} = y_i - y_j ,$$

be used in calculating the “nearest-image” forces between all interacting pairs of particles. This nearest-image distance is calculated by going through the sequence of steps :

$$x_{ij} < -2 \rightarrow x_{ij} = x_{ij} + 4 ; x_{ij} > +2 \rightarrow x_{ij} = x_{ij} - 4 ;$$

$$y_{ij} < -2 \rightarrow y_{ij} = y_{ij} + 4 ; y_{ij} > +2 \rightarrow y_{ij} = y_{ij} - 4 .$$

With the initial and boundary conditions in place, the ensuing dynamics of this system requires the solution of 64 first-order ordinary differential equations :

$$\{ \dot{r}_i = v_i \} ; \{ \dot{v}_i = \sum_j 800r_{ij}(1 - r_{ij}^2)^3 \} ,$$

or, equivalently, 32 second-order differential equations :

$$\{ \ddot{r}_i = \dot{v}_i = \sum_j 800r_{ij}(1 - r_{ij}^2)^3 \} ,$$

where the differential equations for each vector r_i and each vector v_i correspond to pairs of equations for the x and y components of these vectors.

Figure 1.7 shows the time histories of the total, kinetic, and potential energies for two solutions, Runge-Kutta and Leapfrog. In both cases the trajectories were reversed after 12,000 timesteps, with $dt = 0.002$. In the Runge-Kutta case the energy plot is accurate to five digits at $t = 12$. It still appears to be perfectly symmetric about the reversal time (24) even though the final configuration, with a total time of $24+24$, shows coordinate errors and potential/kinetic energy errors of order 0.1 . The apparent symmetry

is illusory. The errors in the Runge-Kutta algorithm are only small, and are *not* time-reversible.

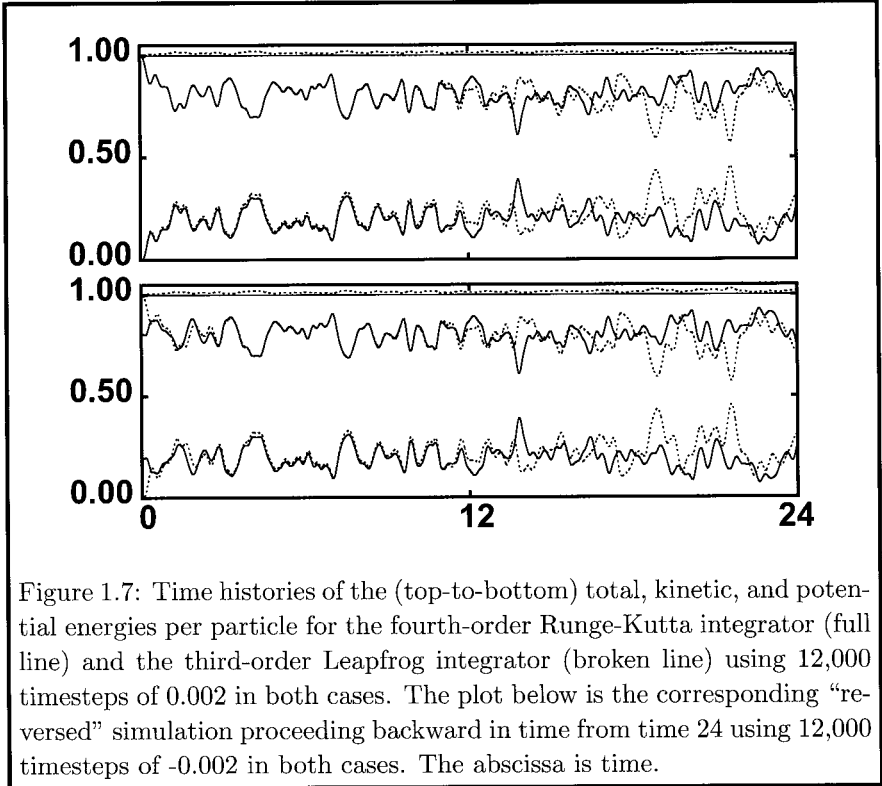


Figure 1.7: Time histories of the (top-to-bottom) total, kinetic, and potential energies per particle for the fourth-order Runge-Kutta integrator (full line) and the third-order Leapfrog integrator (broken line) using 12,000 timesteps of 0.002 in both cases. The plot below is the corresponding “reversed” simulation proceeding backward in time from time 24 using 12,000 timesteps of -0.002 in both cases. The abscissa is time.

In the Leapfrog case the energy and coordinate errors are much larger, with readily visible discrepancies appearing between simulations with dt values of either 0.001 and 0.002 at $t = 12$, the same time at which the leapfrog trajectories deviate visibly from the more-nearly-accurate Runge-Kutta solutions. The leapfrog trajectory *reversibility* is still *nearly* perfect, despite its relatively large trajectory errors. The lack of precise time reversibility for the leapfrog algorithm is due only to computational rounding errors.^{19,20}

The energy errors from either integration scheme can be estimated directly. The classic fourth-order Runge-Kutta scheme, with a timestep

¹⁹Levesque and Verlet (1993).

²⁰Kum and Hoover (1994).

$dt = 0.002$ would ideally incur an error per timestep of the same order as the double-precision computer roundoff error ,

$$\text{error} \simeq (d^5 r / dt^5) dt^5 / 120 \simeq 10^{-15} .$$

But the force law discontinuity (in the third derivative), which comes into play at the beginning and end of every collision, gives a somewhat larger coordinate error Δr , of order

$$F \simeq 6400(\delta r)^3 \longrightarrow \Delta r \simeq \frac{1}{2} 6400(vdt)^3 dt^2 \simeq 10^{-10} .$$

These single-step integration errors, though small, are amplified exponentially fast by the chaotic Lyapunov-unstable many-body dynamics. A comprehensive study of the chaotic dynamics shows that small perturbations grow roughly as $e^{\lambda t}$, where the largest Lyapunov exponent²¹ λ is about 3. Thus a relatively short Runge-Kutta simulation of just 6000 timesteps ($t \rightarrow 12$) is already long enough that the reversed trajectory visibly fails to reproduce the reversed initial configuration.

It is amusing that a much less accurate simulation, a “bit-reversible” leapfrog algorithm described by Levesque and Verlet,

$$r(t + dt) - 2r(t) + r(t - dt) \equiv [(dt)^2 a(t)] ,$$

where all the coordinates, as well as the combination $(dt)^2 a(t)$ are restricted to be single-precision *integers*, regains the initial condition *perfectly*, without any roundoff error at all, despite the inaccuracy of the corresponding trajectory. We will revisit the relatively subtle subject of errors in numerical integration in Chapter 6 .

²¹Hoover and Posch (1995).

1.10 References

- (1) W. H. Press, B. P. Flannery, S. A. Teukolsky, and W. T. Vetterling, *Numerical Recipes, The Art of Scientific Computing* (Cambridge University Press, London, 1986).
- (2) R. A. Gingold and J. J. Monaghan, “Smoothed Particle Hydrodynamics: Theory and Application to Nonspherical Stars”, *Monthly Notices of the Royal Astronomical Society* **181**, 375-389 (1977).
- (3) L. B. Lucy, “A Numerical Approach to the Testing of the Fission Hypothesis”, *The Astronomical Journal* **82**, 1013-1024 (1977).
- (4) J. Gleick, *Chaos, Making a New Science* (Viking, New York, 1989).
- (5) Wm. G. Hoover, *Computational Statistical Mechanics* (Elsevier, New York, 1991). [*Keisan Toukei Rikigaku*, Japanese translation by Koichiro Shida with the supervision of Susumu Kotake (Morikita Shupan, 1999)].
- (6) R. Preston, “Capturing the Unicorn”, *New Yorker Magazine*, 11 April 2005.
- (7) J. B. Gibson, A. N. Goland, M. Milgram, and G. H. Vineyard, “Dynamics of Radiation Damage”, *Physical Review* **120**, 1229-1253 (1960).
- (8) B. J. Alder and T. E. Wainwright, “Molecular Dynamics by Electronic Computers”, pages 97-131 in *Transport Processes in Statistical Mechanics*, I. Prigogine, Editor (Interscience, New York, 1958).
- (9) The “Fermi-Pasta-Ulam” problem is reviewed and extended in J. L. Tuck and M. T. Menzel, “The Superperiod of the Nonlinear Weighted String Problem”, *Advances in Mathematics* **9**, 399-407 (1972).
- (10) Wm. G. Hoover, “Mécanique de Nonéquilibre à la Californienne”, *Physica A* **240**, 1-11 (1997).
- (11) S. Nosé, “Constant Temperature Molecular Dynamics Methods”, *Progress in Theoretical Physics Supplement* **103**, 1-117 (1991).
- (12) Wm. G. Hoover, “Liouville’s Theorems, Gibbs’ Entropy, and Multifractal Distributions for Nonequilibrium Steady States”, *Journal of Chemical Physics* **109**, 4164-4170 (1998).
- (13) J. W. Gibbs, *Elementary Principles in Statistical Mechanics* (Oxbow Press, 1991) [first published in 1902].
- (14) C. Cercignani, *Ludwig Boltzmann, the Man Who Trusted Atoms* (Oxford University Press, 1998).
- (15) B. Moran, W. G. Hoover, and S. Bestiale, “Diffusion in a Periodic Lorentz Gas”, *Journal of Statistical Physics* **48**, 709-726 (1987).
- (16) Wm. G. Hoover and C. G. Hoover, “Searching for Auxetics with Dyna3d and ParaDyn”, *Physica Status Solidi* **242b**, 585-594 (2005).

- (17) C. K. Birdsall and A. B. Langdon, *Plasma Physics via Computer Simulation* (McGraw-Hill, New York, 1985).
- (18) T. J. Ahrens, T. Takata, J. D. O’Keefe, and G. S. Orton, “Impact of Comet Shoemaker-Levy 9 on Jupiter”, *Geophysical Research Letters* **21**, 1087-1090 (1994).
- (19) D. Levesque and L. Verlet, “Molecular Dynamics and Time Reversibility”, *Journal of Statistical Physics* **72**, 519-537 (1993).
- (20) O. Kum and W. G. Hoover, “Time-Reversible Continuum Mechanics”, *Journal of Statistical Physics* **76**, 1075-1081 (1994).
- (21) Wm. G. Hoover and H. A. Posch, “Shear Viscosity *via* Local Control of Spatiotemporal Chaos in Two-Dimensional Isoenergetic Dense Fluids”, *Physical Review E* **51**, 273-279 (1995).